CORE
Metadata, citation and similar papers at core.ac.uk
Provided by Queensland University of Technology ePrints Archive

QUT Digital Repository:
http://eprints.qut.edu.au/

Gudimetla, Prasad and Kharidi, Aprameya and Yarlagadda, Prasad, K.D.V. (2009) ***Simulation of delaminations in composite laminates***. In: Proceedings of the 6th International Conference on Precision, Meso, Micro and Nano Engineering, 11-12 December 2009, Coimbatore, India.

© **Department Of Mechanical Engineering Psg College Of Technology Coimbatore ; Department Of Mechanical Engineering Amrita School Of Engineering Amrita Vishwa Vidyapeetham (University) Coimbatore**

Simulation of delaminations in composite laminates

P.Gudimetla[*], A. Kharidi[+], P.K.D.V. Yarlagadda[#]

[*]Lecturer
School of Engineering Systems
Queensland University of Technology
Brisbane, Australia
Email: p.gudimetla@qut.edu.au

[+]Research Assistant
School of Engineering Systems
Queensland University of Technology
Brisbane, Australia
Email: a.kharidi@qut.edu.au

[#]Director – Smart Systems Theme
School of Engineering Systems
Queensland University of Technology
Brisbane, Australia
Email: y.prasad@qut.edu.au

Abstract: Lamb waves propagation in composite materials has been studied extensively since it was first observed in 1982. In this paper, we show a procedure to simulate the propagation of Lamb waves in composite laminates using a two-dimensional model in ANSYS. This is done by simulating the Lamb waves propagating along the plane of the structure in the form of a time dependent force excitation. In this paper, an 8-layered carbon reinforced fibre plastic (CRFP) is modelled as transversely isotropic and dissipative medium and the effect of flaws is analyzed with respect to the defects induced between various layers of the composite laminate. This effort is the basis for the future development of a 3D model for similar applications.

Keywords: Composites, delamination, Lamb waves, ANSYS

1.0 Introduction

Composite materials are finding increasing use as primary structural components in many modern applications especially in the aerospace industry. However, it is well known that these materials are highly susceptible to hidden internal flaws which may occur during the manufacturing and processing of the material. A major concern is the growth of undetected hidden damage caused by these defects. The current approach of using conventional non-destructive evaluation such as C-scan, radiography, thermography, eddy current etc is expensive, time consuming and often cannot be performed on structures already placed in service because of the inaccessibility or the special equipment required to perform the test.

The integrity, stiffness and durability (residual life) of composite structures need to be determined non-destructively to assure the performance of these structures in service using smaller safety factors. While the integrity and stiffness can be extracted directly from NDE measurements, strength and durability cannot be measured non-destructively since they are associated with physical parameters that cannot be measured with such methods. NDE methods are developed to detect and characterize flaws and to determine the material properties of test specimens. For many years, composites as multi-layered anisotropic media, have posed a challenge to the NDE research community and pulse-echo and through-transmission were the leading methods of determining the quality of composites (Moser, Jacobs and Qu, 1999). However, these methods provide limited and mostly qualitative information about the material properties and defects. The use of lamb waves is potentially an attractive solution since they can propagate over considerable distances. If a receiving transducer is positioned at a remote point on the structure, the received signal contains information about the integrity of the line between the transmitting and receiving transducers. The test therefore monitors a line rather than a point, saving time and money.

Lamb waves produce stresses throughout the plate thickness; therefore surface as well as internal defects can be detected. However, in lamb wave propagation, the vibration patterns through the plate are quite different for different Lamb modes, and are even different for the same mode at different frequencies (Alleyne and Cawley, 1992). Modes at certain frequencies can therefore be selected according to their sensitivity to the defects of interest.

Guo and Cawley (1993) have investigated the possibility of using the S_o mode for the long-range inspection of laminates. They showed that the pulse-echo configuration in which the S_o mode is generated by a transmitting transducer and reflections of the same mode returning to a receiver placed close to the transmitter is the most promising configuration. If there are no defects along the propagation path, no reflection, or only the reflection from the end of the laminate should be received. If there is a defect, an extra reflection from the defect will occur and arrive ahead of that from the end of the laminate. The range of the techniques was found to be limited by the attenuation in the laminate and the signal-to-noise ratio of the transmitter-receiver system used. Their studies show that it is possible to detect delaminations of 10mm in diameter, the minimum size tolerance of a delamination allowed over a range of at least 500mm.

2.0 Material property modeling of anisotropic carbon fibres

Table 1 shows the material properties for a typical carbon fibre reinforced plastic (CFRP). Direction 1 represents the fibre direction while direction 2 is normal to the fibre direction. The carbon fibre is transversely isotropic meaning the material properties are the same in plane (2-3). Thus the stiffness matrix is given by equation (1). The material properties in Table 1 together with equation (1) fully define the properties of unidirectional CFRP.

Table 1: Material properties for unidirectional CFRP.

E_{11} (GPa)	E_{22} (GPa)	G_{12} (GPa)	ν_{12}	ν_{23}	ρ (kg/m^3)
126.6	8.7	3.7	0.32	0.5	1605

$$[C]=\begin{bmatrix} C_{11} & C_{12} & C_{12} & 0 & 0 & 0 \\ C_{12} & C_{22} & C_{23} & 0 & 0 & 0 \\ C_{12} & C_{23} & C_{22} & 0 & 0 & 0 \\ 0 & 0 & 0 & \frac{C_{22}-C_{23}}{2} & 0 & 0 \\ 0 & 0 & 0 & 0 & C_{55} & 0 \\ 0 & 0 & 0 & 0 & 0 & C_{55} \end{bmatrix} \quad \text{.....(1)}$$

$$[C]=\begin{bmatrix} \frac{1-\nu_{23}\nu_{32}}{E_2E_3\Delta} & \frac{\nu_{21}+\nu_{23}\nu_{31}}{E_2E_3\Delta} & \frac{\nu_{31}+\nu_{21}\nu_{32}}{E_2E_3\Delta} & 0 & 0 & 0 \\ \frac{\nu_{21}+\nu_{23}\nu_{31}}{E_2E_3\Delta} & \frac{1-\nu_{13}\nu_{31}}{E_1E_3\Delta} & \frac{\nu_{32}+\nu_{12}\nu_{31}}{E_1E_3\Delta} & 0 & 0 & 0 \\ \frac{\nu_{31}+\nu_{21}\nu_{32}}{E_2E_3\Delta} & \frac{\nu_{32}+\nu_{12}\nu_{31}}{E_1E_3\Delta} & \frac{1-\nu_{12}\nu_{21}}{E_1E_2\Delta} & 0 & 0 & 0 \\ 0 & 0 & 0 & G_{23} & 0 & 0 \\ 0 & 0 & 0 & 0 & G_{31} & 0 \\ 0 & 0 & 0 & 0 & 0 & G_{12} \end{bmatrix} \quad \text{.....(2)}$$

where $\Delta=\left(1-\nu_{12}\nu_{21}-\nu_{23}\nu_{32}-\nu_{13}\nu_{31}-2\nu_{21}\nu_{32}\nu_{13}\right)/\left(E_1E_2E_3\right)$ .....(3)

It should be noted that ν_{12}, ν_{23}, and ν_{13} are the major Poisson's ratios and their corresponding minor Poisson's ratios are related by equation (4) below:

$$\frac{v_{ij}}{E_i} = \frac{v_{ji}}{E_j} \quad \text{.....(4)}$$

Extra care must be taken in determining the Poisson's ratios because cross ply configuration is involved and ANSYS is very particular about the values of major and minor Poisson's ratios. Further, the stiffness matrix in equation (2) must be positive definite, which implies that equation (3) must be positive. Table 2 verifies this condition below.

Table 2: Verification of Positive definite of the Stiffness Matrix

		Major ν		Minor ν	
E11(Fiber)	1.27E+11				
E22	8.70E+09	ν 23	0.5	ν 32	0.5
E33	8.70E+09	ν 13	0.32	ν 31	0.021991
G23	2.90E+09	ν 12	0.32	ν 21	0.021991
G31	3.70E+09				
G12	3.70E+09				
DELTA	7.61E-32				
C22	1.19E+10				
C23	6.05E+09				

2.2 Major and minor Poisson's ratios in ANSYS

In ANSYS, **PRXY**, **PRYZ** and **PRXZ** represent the major Poisson's ratios. For Example, **PRXY** = $-\frac{\varepsilon_y}{\varepsilon_x}$ whereby the force is applied in the *x* direction and contraction occurs in the *y* direction.

2.3 Largest element size used for cross ply model

Apart from accurate material property declaration in the finite element model, the element size is of critical importance since this is determined by the smallest wavelength of the wave which might be present in the cross ply model and can be approximated as $l_e = \frac{\lambda_{\min}}{20}$. The minimum wavelength should correspond to the minimum phase velocity given a constant frequency, as related by $\lambda_{\min} = \frac{v_{\min}}{f}$. Thus, in the cross ply model, the slowest wave is the A0 mode with phase velocity equals to $1.5\,mm/\mu s$. By using the central frequency of 0.5MHz, the smallest wavelength is 3mm. This corresponds to the largest element size of 0.15mm. However, a sensitivity analysis revealed that an element size of 0.20mm can be used without much compromise in the accuracy of the results.

2.4 Largest computational time step

The largest time step is determined by the highest frequency which might present in the cross ply model. As a general rule, $\Delta t = \frac{1}{20 f_{\max}}$. Taking the central frequency of 0.5MHz, $\Delta t = 0.1\mu s$. However, in

some cases such as the input frequency distributes itself over a wide range or the load is stepped up too suddenly, an even smaller time step of ($\Delta t = \frac{1}{180 f_{\max}}$) is required in order to obtain accurate results.

4.0 Finite element modeling of CRFP composite laminate

Using the commercial software ANSYS, a 2D model with delaminations in the cross ply laminate was created as shown in Figure 1. The 8 ply CFRP is 300mm in length and each ply is 0.125mm tick giving an overall thickness of 1 mm. Two idealized defects were created between layers 1&2 and 3&4 respectively to represent local delaminations in between the layers. The defect between layers 1&2 was placed at a distance of 80-mm from the right edge of the composite laminate and was 10 mm in length and 0.05 mm in height while the defect between layers 3&4 was placed at a distance of 160-mm were placed and was of the same length as the first defect but only 0.03 mm in height. Fig. 2 shows the mesh round the delamination. The lower and the upper interfaces of the delamination were represented by coincident nodes which lied along the delamination. The FE mesh used was 8 x 1500, 8 elements across the thickness and 1500 elements along the length.

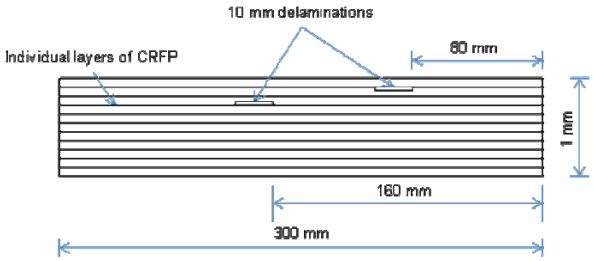

Fig 1 2-dimensional FE model

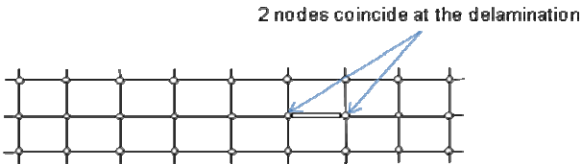

Fig. 2 Meshing around delamination

5.0 Results and Discussion

The first simulation was performed in a zone of no defect in the model and stopped after 1 µs. The input waveform is shown in Fig. 3 while the response is shown in Fig. 4 below as normalized time-displacement waveforms where T_{S0} is the transmitted mode and $R_{S0\text{-}R}$ is the reflected S0 mode from the right end of the composite laminate. The time lag between the T_{S0} and $R_{S0\text{-}R}$ corresponds to the time required for the mode to travel the 300 mm from the middle of the laminate to the end and back. It is noted that $_{S0}$ mode is almost non-dispersive in the frequency-thickness region of 1 MHz-mm.

Fig. 3 Input waveform of Lamb waves

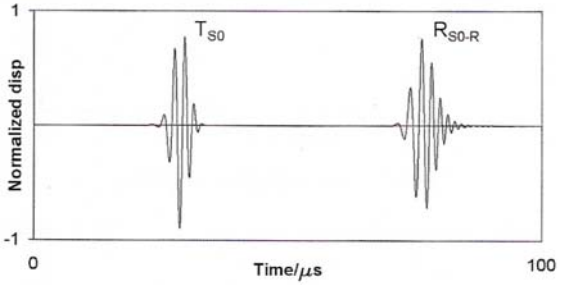

Fig. 4 Observed response undelaminated CRFP

5.1 Delamination under normal shear stress mode

Fig. 5 shows the response wave for a 10-mm long delamination corresponding to Fig. 1 There is an additional reflection ($R_{S0\text{-}D}$) which is the reflected $_{S0}$ mode from the delamination. This signature can be

correlated to the exact location of the delamination in terms of the time taken for the wave to propagate through the composite laminate. A similar signature can be observed in the case of the second delamination between layers 3&4.

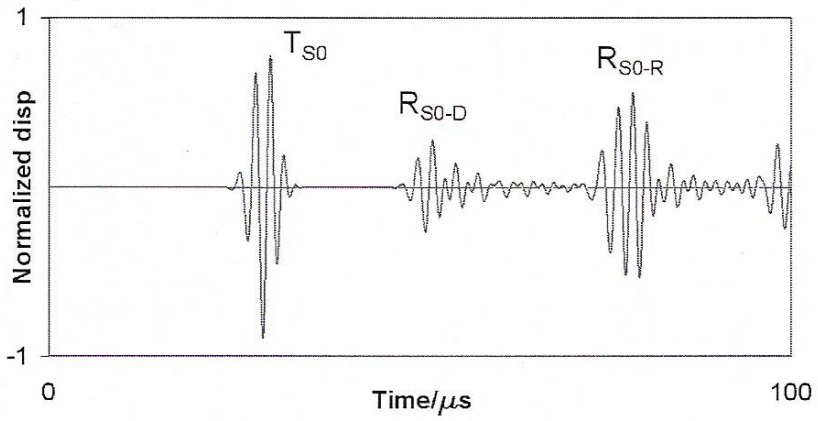

Fig. 5 Observed response of T_{S0}, R_{S0-D} and R_{S0-R} in delaminated CRFP

The transform of the signatures obtained between the no defect zones and the defective zones of the composite laminates of layers 1&2 is shown in Fig. 6 below. It can be seen that the there is a significant drop in the normalized displacement amplitude of the transform of the signature from the defect zone as compared to that from a no defect zone (R_{SO-R}). A similar trend is observed for the defect in layers 3&4 as shown in Figure 7. We performed additional post-processing of the Lamb wave signatures obtained from the two defects within the composite laminate as shown in Figure 8. Although there is a clear and distinct difference in the two waveforms produced by the delaminations in different layers of the composite laminate, determining the position and size of the delamination would be much more difficult and requires other signal processing techniques to smoothen the waveform and isolate into a readable window.

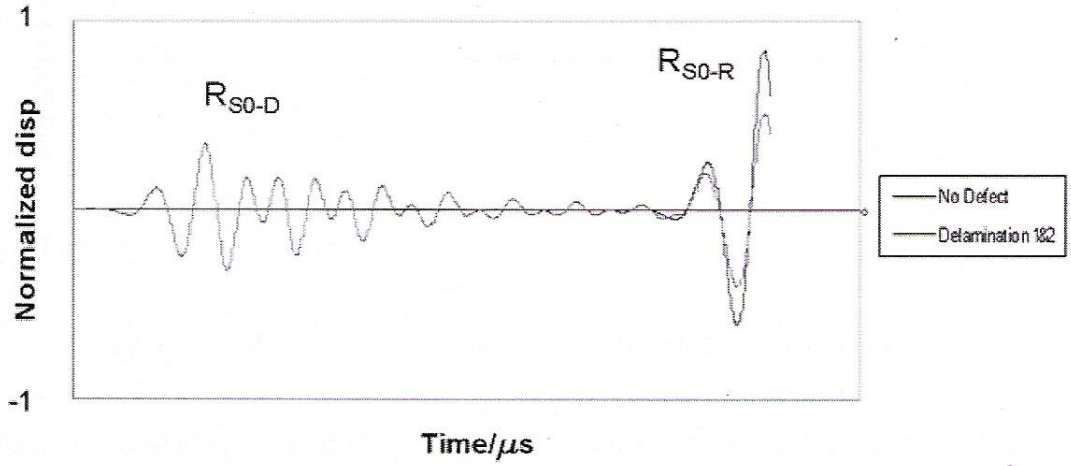

Fig. 6 Comparison of R_{SO-R} dispersion between layers 1 and 2 with a no defect laminate

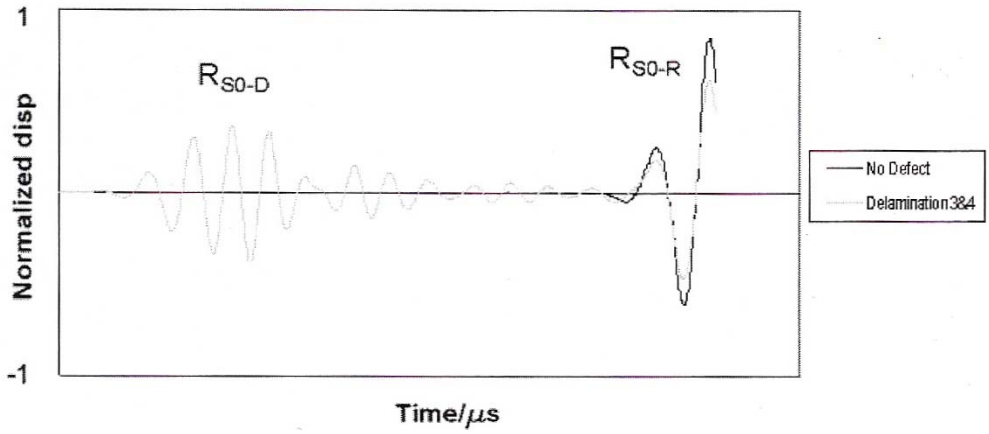

Fig. 7 Comparison of R_{SO-R} dispersion between layers 3-4 with a no defect laminate

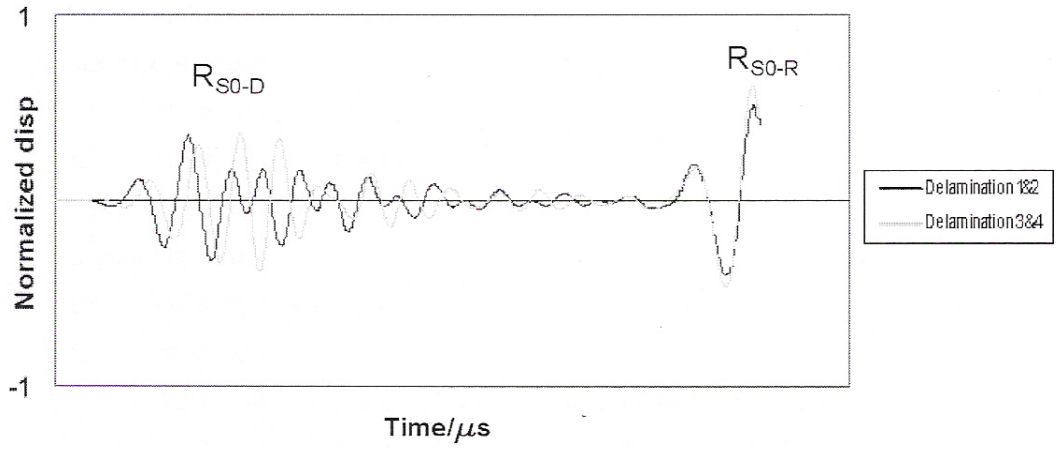

Fig. 8 Comparison of R_{SO-R} dispersion between layers 1-2 and 3-4

6.0 Conclusion

This work has shown that the finite element analysis approach can be used as a convenient method to simulate the propagation of Lamb waves through composite laminates and is being extended to study the defects in a three dimensional model for the purpose of carrying out a stress analysis around defects under high impact loading scenarios.

7.0 References

1. Alleyne, D.N., and Cawley, P., 1992, "The interaction of Lamb waves with defects," IEEE Trans. on Ultrasonics, Ferroelectric and Frequency Control, 39(3), 41-48
2. Guo, N and Cawley, P. 1993, "The interaction of Lamb waves with delaminations in composite laminates, J. Acoustic Soc. Am. 94, pp. 2240-2246
3. Moser, F., Jacobs, L.J., Qu, J. 1999, "Modeling elastic wave propagation in waveguides with the finite element method," 2nd Ed., NDT&E International, 32, pp. 255-264